A dynamical model for correlated two-pion-exchange in the pion-nucleon interaction

C. Schütz, K. Holinde and J. Speth

Institut für Kernphysik, Forschungszentrum Jülich GmbH, D–52425 Jülich, Germany

B.C. Pearce

Dept. of Physics and Math. Physics, The University of Adelaide, Adelaide 5005, Australia

J.W. Durso

Dept. of Physics, Mount Holyoke College, MA 01075

Abstract

A microscopic model for the $N\bar{N} \to \pi\pi$ process is presented in the meson exchange framework, which in the pseudophysical region agrees with available quasiempirical information. The scalar (σ) and vector (ρ) piece of correlated two–pion exchange in the pion–nucleon interaction is then derived via dispersion integrals over the unitarity cut. Inherent ambiguities in the method and implications for the description of pion–nucleon scattering data are discussed.

I. INTRODUCTION

The interaction between a pion and a nucleon plays a prominent role in low and medium energy physics since it is an important ingredient in many other hadronic reactions, *e.g.* pion production in nucleon-nucleon collisions or scattering of a pion by a nucleus.

Recently we have presented a meson exchange model for πNscattering [1] which contains conventional direct and exchange pole diagrams (Fig. 1(a)...1(d)) plus σ– and ρ–exchange terms (Fig. 1(e), (f)), and is unitarized by means of the relativistic Schrödinger equation. The main difference from former models [2–6] is the evaluation of the scalar–isoscalar (σ) and vector–isovector (ρ) terms. While in Refs. [2–6] these contributions are treated as single exchanges with sharp masses, in Ref. [1] they were viewed as arising from a correlated pair of two pions in the J=0 (σ) and J=1 (ρ) t channels (see Fig. 2). Their contribution was evaluated by using quasiempirical information about the t-channel $N\bar{N} \to \pi\pi$ amplitudes of Fig. 2 in the pseudophysical region, which has been obtained by Höhler *et al.* [7] from an analytical continuation of both πN and $\pi\pi$ data, and performing a suitable dispersion integral over the unitarity cut.

In order to build in constraints from soft pion theorems, a subtracted dispersion relation was used in Ref. [1] for the scalar contribution. This leads to a specific feature apparently favored by the πN data: namely, the resulting interaction is repulsive in S waves but attractive in P waves. The approach used in Ref. [1] led to a considerably stronger contribution from ρ exchange than used in former treatments. On the other hand, by defining effective coupling constants suitable for a sharp ρ–mass parametrization we found a rather small tensor to vector ratio of coupling strengths in the physical t region, in line with values used before in the πN system [2].

As shown in Ref. [1], a model based on the diagrams of Figs. 1 and 2 results in πN phase shifts in the elastic region that agree well with empirical information, as do the scattering lengths and the πN Σ-term (≈ 65MeV).

Although the approach outlined above and described in detail in Ref. [1] for evaluating

correlated 2π-exchange is certainly adequate for free πN scattering, problems arise when this πN interaction is used in other areas of physics. For example, modifications of the interaction in the nuclear medium, which come into play when a pion is scattered by a nucleus, cannot be taken into account. The study of such effects requires an explicit field-theoretic description.

The aim of the present work is to provide such an explicit model for the correlated 2π- and $K\bar{K}$-exchange process of Fig. 2. This requires as input realistic $\pi\pi \to \pi\pi$ and $\pi\pi \to K\bar{K}$ T matrices, which we have generated from a potential model based similarly on meson exchange and involving coupling between $\pi\pi$ and $K\bar{K}$ channels (see Fig. 3). The use of such a dynamical model for the $\pi\pi$ interaction will facilitate future investigation of not only possible medium modifications of the pion and nucleon legs, but also of the interaction itself.

The paper is organized as follows: In the next section, the microscopic model for the $N\bar{N} \to 2\pi$ process is described and compared to the data in the pseudophysical region. Section III deals with the resulting pion–nucleon interaction terms arising from correlated 2π exchange and their implications for the description of empirical πN data. Section IV contains a short summary and outlook.

II. MICROSCOPIC MODEL FOR THE $N\bar{N} \to \pi\pi$ PROCESS

We will generate the amplitude for the process of Fig. 2 by solving the scattering equation

$$T_{N\bar{N}\to\pi\pi} = V_{N\bar{N}\to\pi\pi} + \sum_{pp=\pi\pi,K\bar{K}} T_{pp\to\pi\pi} g_{pp} V_{N\bar{N}\to pp} \tag{2.1}$$

Here $V_{N\bar{N}\to pp}$ is the transition interaction and $T_{pp\to\pi\pi}$ the transition amplitudes from $\pi\pi$ and $K\bar{K}$ to $\pi\pi$; both will be specified below (we use p to denote a generic pseudoscalar meson, π, K or $\bar{K}$). Eq. (2.1) could be considered to be a four-dimensional Bethe-Salpeter-type equation. However, we use the Blankenbecler-Sugar (BbS) technique [8] to reduce the dimensionality of the integral to three, which simplifies the calculation while maintaining unitarity. More explicitly, we have, in the c.m. system and in the helicity representation,

$$\langle \vec{q}\,00|T_{N\bar{N}\to\pi\pi}(t)|\vec{p}\,\lambda_N\lambda_{\bar{N}}\rangle = \langle \vec{q}\,00|V_{N\bar{N}\to\pi\pi}(t)|\vec{p}\,\lambda_N\lambda_{\bar{N}}\rangle$$
$$+\sum_{pp}\int d^3k\,\frac{\langle \vec{q}\,00|T_{pp\to\pi\pi}(t)|\vec{k}\;00\rangle\langle \vec{k}\,00|V_{N\bar{N}\to pp}(t)|\vec{p}\,\lambda_N\lambda_{\bar{N}}\rangle}{(2\pi)^3\omega_p(k)(t-4\omega_p^2(k))} \tag{2.2}$$

with

$$\omega_p(k) = \sqrt{k^2+m_p^2}\ , \tag{2.3}$$

where $m_p = m_\pi, m_K$ for $p = \pi, K$ respectively. Thus, k is the magnitude of the three-momentum part $\vec{k}$ of the relative four-momentum of the intermediate two-meson state. The four-momenta of the two intermediate mesons k_1 and k_2 are related to $\vec{k}$ by

$$k_1 = \left(\sqrt{t}/2, \vec{k}\right)$$
$$k_2 = \left(\sqrt{t}/2, -\vec{k}\right) \tag{2.4}$$

The helicity of the nucleon (antinucleon) is denoted by λ_N ($\lambda_{\bar{N}}$). We perform a partial wave decomposition by writing

$$\langle \vec{q}\,00|V_{N\bar{N}\to pp}(t)|\vec{p}\,\lambda_N\lambda_{\bar{N}}\rangle = \frac{1}{4\pi}\sum_J (2J+1)d^J_{\lambda 0}(\cos\theta)\langle 00|V^J_{N\bar{N}\to pp}(q,p;t)|\lambda_N\lambda_{\bar{N}}\rangle \tag{2.5}$$

with a similar expression for $T_{N\bar{N}\to\pi\pi}$. Here, $d^J_{\lambda 0}$ are the conventional reduced rotation matrices, θ is the angle between $\vec{p}$ and $\vec{q}$, and $\lambda = \lambda_N - \lambda_{\bar{N}}$. Using these expressions, Eq. (2.2) becomes

$$\langle 00|T^J_{N\bar{N}\to\pi\pi}(q,p;t)|\lambda_N\lambda_{\bar{N}}\rangle = \langle 00|V^J_{N\bar{N}\to\pi\pi}(q,p;t)|\lambda_N\lambda_{\bar{N}}\rangle$$
$$+\sum_{pp}\int_0^\infty dk\,k^2\,\frac{\langle 00|T^J_{pp\to\pi\pi}(q,k;t)|00\rangle\langle 00|V^J_{N\bar{N}\to pp}(k,p;t)|\lambda_N\lambda_{\bar{N}}\rangle}{(2\pi)^3\omega_p(k)(t-4\omega_p^2(k))} \tag{2.6}$$

The $N\bar{N}\to 2\pi$ on-shell amplitudes are related to the Frazer-Fulco helicity amplitudes $f^J_\pm$ [9] via

$$f^J_+(t) = \frac{p_{on}m_N}{4(2\pi)^2(p_{on}q_{on})^J}\langle 00|T^J_{N\bar{N}\to\pi\pi}(q_{on},p_{on};t)|\tfrac{1}{2}\tfrac{1}{2}\rangle$$
$$f^J_-(t) = -\frac{p_{on}m_N}{2(2\pi)^2\sqrt{t}(p_{on}q_{on})^J}\langle 00|T^J_{N\bar{N}\to\pi\pi}(q_{on},p_{on};t)|\tfrac{1}{2}(-\tfrac{1}{2})\rangle \tag{2.7}$$

with

$$q_{on} = \sqrt{\frac{t}{4} - m_\pi^2}$$
$$p_{on} = \sqrt{\frac{t}{4} - m_N^2} \quad . \tag{2.8}$$

A. The $N\bar{N} \to \pi\pi, K\bar{K}$ transition potentials

The ingredients of the dynamical model for the transition interactions $V_{N\bar{N}\to\pi\pi}$ and $V_{N\bar{N}\to K\bar{K}}$ employed in this paper are displayed graphically in Fig. 4. The potential $V_{N\bar{N}\to\pi\pi}$ ($V_{N\bar{N}\to K\bar{K}}$) consists of N and Δ (Λ and Σ) exchange terms plus ρ–meson pole diagrams. Their evaluation is based on the following spin-momentum dependent parts of the interaction Lagrangians

$$\mathcal{L}_{BBp} = \frac{f_{BBp}}{m_p} \bar{\psi}_B \gamma^5 \gamma^\mu \psi_B \partial_\mu \phi_p \tag{2.9a}$$

$$\mathcal{L}_{NN\rho} = g_{NN\rho} \bar{\psi}_N \gamma^\mu \psi_N \phi_{\rho,\mu} + \frac{f_{NN\rho}}{4m_N} \bar{\psi}_N \sigma^{\mu\nu} \psi_N \left(\partial_\mu \phi_{\rho,\nu} - \partial_\nu \phi_{\rho,\mu}\right) \tag{2.9b}$$

$$\mathcal{L}_{N\Delta\pi} = \frac{f_{N\Delta\pi}}{m_\pi} \bar{\psi}^\mu_\Delta \left(g_{\mu\nu} + x_\Delta \gamma_\mu \gamma_\nu\right) \psi_N \partial_\mu \phi_\pi \quad + \quad H.c. \tag{2.9c}$$

$$\mathcal{L}_{\rho pp} = g_{\rho pp} \phi_p \phi^\mu_\rho \partial_\mu \phi_p \tag{2.9d}$$

Here, ψ_B are the field operators for spin-1/2 particles (N, Λ, Σ), ψ_Δ is the spin-3/2 Δ-isobar operator, ϕ_p are the corresponding operators for pseudoscalar (π, K) mesons, while ϕ_ρ denotes the ρ meson. Also, $\sigma^{\mu\nu} = \frac{i}{2}[\gamma^\mu, \gamma^\nu]$. The $N\Delta\pi$ coupling (Eq. (2.9c)) includes off-mass-shell contributions, whose strength is characterized by the parameter x_Δ. For the propagators, we have

$$S_B(p) = \frac{\not{p} + m_B}{p^2 - m_B^2} \tag{2.10a}$$

$$S^{\mu\nu}_\Delta(p) = \frac{\not{p} + m_\Delta}{p^2 - m_\Delta^2} \left[-g^{\mu\nu} + \frac{1}{3}\gamma^\mu\gamma^\nu + \frac{2}{3m_\Delta^2} p^\mu p^\nu - \frac{1}{3m_\Delta}\left(p^\mu\gamma^\nu - p^\nu\gamma^\mu\right)\right] \tag{2.10b}$$

$$S_\rho^{\mu\nu}(p) = \frac{-g^{\mu\nu} + \frac{p^\mu p^\nu}{m_\rho^2}}{p^2 - m_\rho^2} \tag{2.10c}$$

In this work, we omit the non-pole contributions to the spin-3/2 propagator (Eq. (2.10b) since it is known [10] that their effect can be taken into account by the second term of the interaction Lagrangian (Eq. (2.9c))

As usual, the resulting vertex functions are modified by phenomenological form factors F to account for the extended vertex structure. For the baryon exchange diagrams in Fig. 4 we choose

$$F_{BBp}(q^2) = \left(\frac{n_{BBp}\Lambda_{BBp}^2 - m_B^2}{n_{BBp}\Lambda_{BBp}^2 - q^2} \right)^{n_{BBp}} \tag{2.11}$$

where m_B (q) is the mass (four-momentum) of the exchanged baryon (in the BbS framework adopted here, $q^2 = -\vec{q}^{\,2}$). The cutoff masses Λ_{BBp} and powers n_{BBp} will be adjusted later. For the ρ–pole diagrams we introduce form factors at the meson-meson-meson vertices as follows

$$\begin{aligned} F_{pp\rho}(q) &= \left(\frac{n_{pp\rho}\Lambda_{pp\rho}^2 + m_\rho^2}{n_{pp\rho}\Lambda_{pp\rho}^2 + 4\omega_p^2(q)} \right)^{n_{pp\rho}} \\ &= \left(\frac{n_{pp\rho}\bar{\Lambda}_{pp\rho}^2 - m_p^2 + \frac{m_\rho^2}{4}}{n_{pp\rho}\bar{\Lambda}_{pp\rho}^2 + \vec{q}^{\,2}} \right)^{n_{pp\rho}} \end{aligned} \tag{2.12}$$

with

$$\bar{\Lambda}_{pp\rho} = \left(\frac{\Lambda_{pp\rho}^2}{4} + \frac{m_p^2}{n_{pp\rho}} \right)^{1/2} \tag{2.13}$$

In order to judge the behavior of these form factors it is $\bar{\Lambda}_{pp\rho}$ which should be compared with Λ_{BBp} of Eq. (2.11) or the conventional monopole cutoff parameters.

The evaluation of the relevant transition potentials based on Eqs. (2.9)–(2.12) is involved but straightforward. The resulting expressions have to be multiplied by appropriate isospin factors derived from SU(3). More details can be found in Ref. [11]. Some slight modifications occur since we now use the BbS framework.

B. The $\pi\pi \to \pi\pi, K\bar{K}$ amplitude

The starting point for the evaluation of $T_{\pi\pi\to\pi\pi}$ and $T_{K\bar{K}\to\pi\pi}$ are the driving terms shown in Fig. 3. Such a model, involving the coupled channels $\pi\pi$ and $K\bar{K}$ was constructed by our group some time ago [12] based on time-ordered perturbation theory. Here we use a model with essentially the same physical input, which alternatively uses the BbS technique. This procedure proved to be advantageous when studying the scalar form factor of the pion, kaon and nucleon [13] since it has the correct analytic behavior in the unphysical region (below the $\pi\pi$ threshold). The interaction Lagrangians used are (again without isospin)

$$\mathcal{L}_{\epsilon pp} = \frac{g_{\epsilon pp}}{2m_p}\phi_\epsilon \partial_\mu \phi_p \partial^\mu \phi_p \tag{2.14a}$$

$$\mathcal{L}_{vpp} = g_{vpp}\phi_p \phi_v^\mu \partial_\mu \phi_p \tag{2.14b}$$

$$\mathcal{L}_{f_2pp} = g_{f_2pp}\frac{2}{m_p}\phi_T^{\mu\nu}\partial_\mu\phi_p\partial_\nu\phi_p \tag{2.14c}$$

where v denotes the vector mesons ω, ρ, ϕ and K^* while f_2 is the tensor meson. As before, form factors are attached to each vertex. For t– (s–) channel exchanges, form factors of the form given in Eq. (2.11) (Eq. (2.12)) are used. For the s–channel pole diagrams in our interaction model, bare masses have to be used. These pole contributions then get renormalized to reproduce the physical resonance parameters by the iteration in the scattering equation. Values for bare masses, coupling constants (with some constraints from SU(3) symmetry) and cutoff masses have been adjusted to reproduce the empirical $\pi\pi$ phase shifts and inelasticities. These parameters are given in Tables I — IV. The description of the data is as successful as in Ref. [12]. Fig. 5 shows the phases for the J=0,1 partial waves of relevance in this paper, as well as the S–wave inelasticity around 1 GeV .(In P-waves, the inelasticity is rather small in this energy region.)

C. The model in the pseudophysical region

In order to evaluate the $N\bar{N} \to \pi\pi$ amplitudes it remains to specify the parameters in the $N\bar{N} \to \pi\pi, K\bar{K}$ transition potentials. Masses and most coupling constants are not treated as fit parameters but are taken from other sources, using SU(3) symmetry arguments wherever possible. The ρNN coupling $f^{(0)}_{NN\rho}$ is taken to be equal to the $\rho\pi\pi$ coupling. The parameter x_Δ (Eq. (2.9c)), the bare tensor/vector coupling constant ratio $\kappa^{(0)}_\rho \equiv f^{(0)}_{NN\rho}/g^{(0)}_{NN\rho}$ and the cutoff masses $\Lambda_{NN\pi}$, $\Lambda_{N\Delta\pi}$ have been adjusted to the quasiempirical results obtained by Höhler *et al.* [7] from analytic continuation of πN and $\pi\pi$ data. The values used for the baryon exchange contributions are given in Table V. The value used for $\kappa^{(0)}_\rho$ is 4.136. Note that the functional form of the form factors has been chosen such that the dependence on the power n is quite weak (the factor n multiplying Λ^2 in Eqs. (2.11) and (2.12) ensures an expansion of $F(q^2)/F(0)$ in powers of q^2 is independent of n up to order q^2). We take $n_{NN\pi}$ ($n_{N\Delta\pi}$) to be 1 (2). Since the influence of the $K\bar{K}$ intermediate state is small anyhow, $\Lambda_{N\Lambda K}$ and $\Lambda_{N\Sigma K}$ are arbitrarily put to 2.5 GeV. This rather large value implies that the $K\bar{K}$ contribution as evaluated here is probably an upper limit. For consistency, the parameters at the $\rho\pi\pi$ and $\rho K\bar{K}$ vertex are taken to be the same as in the $\pi\pi \to \pi\pi, K\bar{K}$ model described in the last section.

We mention that the baryon–baryon–meson form factor parameters should not be expected to agree with values employed in the Bonn potential [14] and its extension to the hyperon–nucleon case [15]. The reason is that for the t–channel baryon exchange process considered here, one is in a quite different kinematic regime. The fact that we cannot establish a definite relation for the cutoff parameters in different kinematic domains is the price we have to pay for our simplified treatment of the vertex structure, which makes the form factor depend on the momentum of only one particle. This is a general problem, which, in our opinion, is difficult to avoid, since a reliable QCD calculation of the full momentum dependence of the vertex does not exist.

There is one amplitude, f^0_+, for the scalar (σ) channel whereas there are two, f^1_+ and

f_-^1, for the vector (ρ) channel. In Fig. 6 we show the results in the pseudophysical region ($t \geq 4m_\pi^2$) obtained from our dynamical model, for both the real and imaginary parts.

Given that we have only four free parameters ($\kappa_\rho^{(0)}$, x_Δ, $\Lambda_{NN\pi}$ and $\Lambda_{N\Delta\pi}$), there is remarkable agreement with the quasiempirical result [7] in all amplitudes. Some disagreement occurs in the scalar amplitude, especially at higher t. Fortunately, as we will demonstrate below, these do not severely affect our final result, the correlated $\pi\pi$ (and $K\bar{K}$) exchange potential in πN scattering. Furthermore one should keep in mind that the quasiempirical result is subject to considerable uncertainty at large values of t.

III. πN INTERACTION ARISING FROM CORRELATED 2π EXCHANGE

In order to derive the effective σ– and ρ–exchange potentials we use the same procedure as in Ref. [1]; namely, we first perform dispersion integrals over the unitarity cut using as input the $N\bar{N} \to \pi\pi$ amplitudes derived in the foregoing section. Corresponding πN potentials are then obtained in a straightforward way. We refer the reader to Ref. [1] for details.

A. The potential in the scalar channel

Here, a subtracted dispersion relation is used to impose the chiral symmetry constraint at the Cheng–Dashen point, with $\tilde{f}_+^0(2m_\pi^2)$ put to zero; i.e.

$$\frac{\tilde{f}_+^0(t)}{t-4m_N^2} = \frac{t-2m_\pi^2}{\pi}\int_{4m_\pi^2}^{t_c} \frac{\mathrm{Im}f_+^0(t')}{(t'-t)(t'-4m_N^2)(t'-2m_\pi^2)}\,dt' \tag{3.1}$$

with $t_c = 50m_\pi^2$. Due to the slightly different Imf_+^0 predicted by the dynamical model compared to the pseudoempirical data of Ref. [7] (see Fig. 6) the resulting potential is now a bit stronger compared to that obtained in Ref. [1]. This is demonstrated in Fig. 7, for the on–shell case and some selected partial waves.

B. The potential in the vector channel

As in Ref. [1] we first start from

$$\tilde{f}^1_\pm(t) = \frac{1}{\pi}\int_{4m_\pi^2}^{t_c} \frac{\mathrm{Im} f^1_\pm(t')}{t'-t}\,dt' \quad . \tag{3.2}$$

As expected from the excellent agreement of our model amplitudes $f^1_\pm$ with the quasiempirical ones of Ref. [7] (cp. again Fig. 6), the present results for the πN potential in the ρ–channel are practically the same as those obtained in Ref. [1].

However, it was already pointed out in Ref. [1] that there is a considerable ambiguity in this result. Alternatively, we could have used a method proposed by Frazer and Fulco [9] and applied by Höhler and Pietarinen [16]. Here, one first constructs combinations $\Gamma_{1,2}(t)$ corresponding to vector (Γ_1) and tensor (Γ_2) coupling amplitudes

$$\Gamma_1(t) = -\frac{m_N}{p^2_{on}}\left(f^1_+(t) - \frac{t}{4\sqrt{2}m_N} f^1_-(t)\right) \tag{3.3a}$$

$$\Gamma_2(t) = \frac{m_N}{p^2_{on}}\left(f^1_+(t) - \frac{m_N}{\sqrt{2}} f^1_-(t)\right), \tag{3.3b}$$

and then performs the dispersion integrals over the unitarity cut,

$$\tilde{\Gamma}_{1,2}(t) = \frac{1}{\pi}\int_{4m_\pi^2}^{t_c} \frac{Im\Gamma_{1,2}(t')}{t'-t}dt' \quad . \tag{3.4}$$

Differences in the resulting potentials originate from the additional t–dependence in $\Gamma_{1,2}$ compared to $f^1_\pm$. Despite this fact, since $\Gamma_{1,2}$ have the same analytic structure as $f^1_\pm$, both methods would in principle lead to the same results provided all cut contributions would be taken into account in the dispersion integrals. Indeed, diagrams included in correlated two–pion exchange also give rise to left hand cuts. In the example shown in Fig. 8 the $N\rho$ intermediate state is the source of a branch cut in the complex t plane extending from $-\infty$ to $\simeq -70.5 m_\pi^2$. In fact, there is an infinite number of such left hand cuts generated by all processes contributing to correlated correlated two–pion exchange and it is by far impossible to include these pieces. Anyhow, ρ–exchange is *defined* by the integral over the

unitarity cut only. Therefore it is unavoidable that the results induced by Eqs. (3.2) and (3.4), respectively, will differ. (Cutting off the integration over the unitarity cut at t_c turns out to play a minor role only.)

These differences can be nicely demonstrated by parametrizing the resulting potentials in terms of effective t–dependent ρ–coupling strengths $g_{1,2}(t)$ defined by

$$g_{1,2}(t) = 12\pi(m_\rho^2 - t)\Gamma_{1,2}(t) \quad , \tag{3.5}$$

where $\Gamma_{1,2}$ is either obtained by inserting $\tilde{f}_\pm^1$ calculated using Eq. (3.2) into Eqs. (3.3) or alternatively by dispersing $\Gamma_{1,2}$ (cf. Eq. (3.4)). (For the motivation of the definition of $g_{1,2}$, see Ref. [1].) In Fig. 9 we have plotted the effective vector coupling strength $g_1(t)/4\pi$, the effective tensor coupling strength $g_2(t)/4\pi$ and their ratio $\kappa = \frac{g_2}{g_1}$, choosing m_ρ=770 MeV. Since the t–dependence in p_{on}^2 of Eq. (3.3) is rather weak, the resulting g_2 does not differ much. But the factor of t in Γ_1 leads to a much smaller g_1 if $\Gamma_{1,2}$ are dispersed.

C. Implications for πN scattering

Our model for correlated 2π exchange is supplemented by direct and exchange pole diagrams involving the nucleon and Δ–isobar, and is then unitarized by means of a relativistic Schrödinger equation. We refer to Ref. [1] for details. It has been shown in that paper that, based on the quasiempirical input for the $N\bar{N} \to \pi\pi$ process, a good description of all πN partial waves is obtained by adjusting open form factor parameters. In that paper, ρ exchange as defined by Eqs. (3.2) has been used.

We first want to discuss what happens when we now replace the quasiempirical input for correlated 2π exchange by our dynamical model. The slight increase in the σ–channel potential (Fig. 7) leads to comparably weakly modified phase shifts. This effect can be compensated by a small readjustment of the cutoff parameter (introduced in addition for the σ potential, see Ref. [1]), from 1200 MeV to 1120 MeV. There is almost no change in the ρ channel provided the same ansatz is used as in Ref. [1]. Therefore a quantitative

description of S and P waves is obtained with precisely the same values for parameters in pole and exchange diagrams as in Ref. [1] (solid lines in Fig. 10). Corresponding scattering lengths and volumes are given in Table VI.

However, a dramatic change occurs if the ρ–exchange potential is evaluated using Eq. (3.4). There is a strong reduction in the S_{11} phase shift predictions, with smaller modifications in other partial waves (dashed lines of Fig. 10). The latter can be eliminated by suitably readjusting parameters in the pole and exchange diagrams, but the discrepancy in S_{11} essentially remains.

In view of this situation, one may ask if the πN data can discriminate between the different formulations for ρ exchange. Within the strict confines of our model, it could be argued that it does. On the other hand, the discrepancy could be an indicator of the absence of an important ingredient still missing in the S_{11} interaction. Indeed, there is empirically well–established resonant structure in that partial wave at higher energies, which cannot be reproduced by either model. One source for the required additional attraction in S_{11} is the strong coupling of this partial wave to the reaction channel ηN. A second source of attraction is provided by N^*_{S11} (1535, 1650) pole diagrams in the πN interaction. If direct coupling of the form

$$\mathcal{L}_{N^*N\pi} = g_{N^*N\pi}\bar{\Psi}_{N^*}\vec{\tau}\Psi_N\vec{\Phi}_\pi + H.c. \tag{3.6}$$

is assumed at the $N^*N\pi$ vertex this process gives rise to attraction in the S_{11} partial wave of πN scattering starting from the πN threshold.

To demonstrate the power of these additional degrees of freedom, in Fig. 11 the result of a simple calculation starting from the second model for ρ exchange is plotted where an additional N^* pole diagram has been included. (The parameters used here are: $m^0_{N^*}$=1550 MeV, $(g^{(0)}_{N^*N\pi})^2/4\pi = 0.1$, $\Lambda_{N^*} = 2000$ MeV with the form factor parametrization of Ref. [1].) Obviously such a model can describe low energy πN scattering. Therefore, to discard the second model of ρ exchange on the basis of the current discrepancies is certainly not justified.

IV. SUMMARY

We have presented a dynamical model for the $N\bar{N} \to \pi\pi$ process in the meson exchange framework, which in the pseudophysical region agrees with available quasiempirical information. The scalar (σ) and vector (ρ) piece of correlated two–pion exchange in the pion–nucleon interaction is then derived via a dispersion integral over the unitarity cut. Concerning ρ exchange, there is a sizeable ambiguity in the prediction for its effective strength, which is due to different formulations of the coupling to the nucleon. While the restricted low–energy model we have used favors one formulation, mechanisms such as coupling to the ηN channel and inclusion of higher N^* resonances, not treated in our model but necessary to explain the data at higher energies, could significantly alter this result, and suggest a direction of future investigation.

REFERENCES

[1] C. Schütz, J. W. Durso, K. Holinde, and J. Speth, Phys. Rev. C **49**, 2671 (1994).

[2] B. C. Pearce and B. K. Jennings, Nucl. Phys. **A528**, 655 (1991).

[3] C. Lee, S. N. Yang, and T.-S. H. Lee, J. Phys. **G17**, L131 (1991).

[4] F. Gross and Y. Surya, Phys. Rev. C **47**, 703 (1993).

[5] P. F. A. Goudsmit, H. J. Leisi, and E. Matsinos, Phys. Lett. B **299**, 6 (1993).

[6] P. F. A. Goudsmit, H. J. Leisi, E. Matsinos, B. L. Birbrair, and A. B. Gridnev, Nucl. Phys. **A575**, 673 (1994).

[7] G. Höhler, in *Pion-Nucleon Scattering*, Vol. I/9b2 of *Landolt-Börnstein*, edited by H. Schopper (Springer-Verlag, New York, 1983).

[8] R. Blankenbecler and R. Sugar, Phys. Rev. **142**, 1051 (1966).

[9] W. R. Frazer and J. R. Fulco, Phys. Rev. **117**, 1603 (1960),
W. R. Frazer and J. R. Fulco, Phys. Rev. **117**, 1603 (1960 .

[10] B. J. Read, Nucl. Phys. **B52**, 565 (1973).

[11] T. Hippchen, J. Haidenbauer, K. Holinde, and V. Mull, Phys. Rev. C **44**, 1323 (1991).

[12] D. Lohse, J. W. Durso, K. Holinde, and J. Speth, Nucl. Phys. **A516**, 513 (1990).

[13] B. C. Pearce, K. Holinde, and J. Speth, Nucl. Phys. **A541**, 663 (1992).

[14] R. Machleidt, K. Holinde, and C. Elster, Phys. Rep. **149**, 1 (1987).

[15] B. Holzenkamp, K. Holinde, and J. Speth, Nucl. Phys. **A500**, 485 (1989).

[16] G. Höhler and E. Pietarinen, Nucl. Phys. **B95**, 210 (1975).

[17] G. Höhler, F. Kaiser, R. Koch, and E. Pietarinen, *Handbook of Pion-Nucleon Scattering*, Vol. 12–1 of *Physics Data* (Fachinformationszentrum, Karlsruhe, 1979).

[18] R. Koch and E. Pietarinen, Nucl. Phys. **A336**, 331 (1980).

FIGURES

FIG. 1. Diagrams included in the πN potential.

FIG. 2. Correlated $\pi\pi$ ($K\bar{K}$) exchange contributions.

FIG. 3. The contributions to the potential of the coupled channel $\pi\pi - K\bar{K}$ model.

FIG. 4. The ingredients of the $N\bar{N} \to \pi\pi, K\bar{K}$ transition potentials

FIG. 5. $\pi\pi$ phase shifts obtained for $J = 0$ and $J = 1$ from our coupled channel $\pi\pi - K\bar{K}$ model and the S–wave inelasticity. For references to the data, see Ref. [12].

FIG. 6. $N\bar{N} \to \pi\pi$ helicity amplitudes in the pseudophysical region. The solid lines denote the imaginary parts of the model amplitudes and the dashed lines the real parts. Squares and triangles denote the quasiempirical amplitudes taken from Ref. [7].

FIG. 7. On–shell potentials in various πN partial waves arising from correlated 2π exchange in the scalar channel. The solid lines are the result if the input from the dynamical model is used, the dashed lines are based on the pseudoempirical input given in [17].

FIG. 8. A diagram contributing to correlated two–pion exchange and its cuts.

FIG. 9. Effective coupling strengths for ρ exchange: (a) vector coupling strength $g_1/4\pi$, (b) tensor coupling strength $g_2/4\pi$, (c) $\kappa = g_2/g_1$. The solid lines denote the results if the dispersion integrals are performed for the f amplitudes (Eq. (3.2)); the dashed lines show the results if the form factors $\Gamma_{1,2}$ are dispersed (Eq. (3.4)).

FIG. 10. πN scattering phase shifts in S and P waves, as functions of the pion laboratory momentum. The solid lines originate from the model using the first ansatz for ρ exchange (Eq. (3.2)), the dashed lines denote the results if the second ansatz is used (Eq. (3.4)). Empirical information is taken from Ref. [18].

FIG. 11. S_{11} wave πN phase shift, as function of the pion laboratory momentum. The solid and dashed lines denote the same models as in Fig. 10. The dash–dotted line gives the result if an additional $N^*(S_{11})$ pole is implemented in the model based on Eq. (3.4). Empirical information is taken from Ref. [18].

TABLES

TABLE I. Masses used throughout the calculation in MeV. Bare masses (denoted by the (0) superscript) appear in the s-channel meson exchanges. Isospin-averaged masses are used when appropriate.

Particle	Mass	Particle	Mass	Particle	Mass
π	139.57	$\rho^{(0)}$	1151.3	$f_2^{(0)}$	1710.0
K	495.82	ω	782.6	N	938.926
ϵ	1400.0	K^*	895.0	Δ	1232.0
$\epsilon^{(0)}$	1505.0	ϕ	1020.0	Λ	1115.6
ρ	770.0	f_2	1270.0	Σ	1193.0

TABLE II. Parameters used in the $\pi\pi \to \pi\pi$ potential.

Vertex	Coupling Constant	Form factor power	Cutoff
$\alpha\beta\gamma$	$\frac{g^2_{\alpha\beta\gamma}}{4\pi}$	$n_{\alpha\beta\gamma}$	$\Lambda_{\alpha\beta\gamma}$ (MeV)
$\pi\pi\rho$, t–channel ρ exch.	2.1	2	1650
$\pi\pi\rho$, s–channel ρ exch.	2.1	2	3300
$\pi\pi\epsilon$, s–channel ϵ exch.	0.004	2	2000
$\pi\pi f_2$, s–channel f_2 exch.	0.040	2	2000

TABLE III. Parameters used in the $\pi\pi \to K\bar{K}$ potential.

Vertices	Coupling Constant	Form factor power	Cutoff
$\alpha\beta\gamma$, $\alpha'\beta'\gamma$	$\frac{g_{\alpha\beta\gamma}g_{\alpha'\beta'\gamma}}{4\pi}$	$n_{\alpha\beta\gamma} = n_{\alpha'\beta'\gamma}$	$\Lambda_{\alpha\beta\gamma} = \Lambda_{\alpha'\beta'\gamma}$ (MeV)
$\pi\bar{K}K^*$,$\pi K\bar{K}^*$, t–channel K^* exch.	0.525	2	1800
$\pi\pi\rho$,$K\bar{K}\rho$, s–channel ρ exch.	1.050	2	3300
$\pi\pi\epsilon$,$K\bar{K}\epsilon$, s–channel ϵ exch.	0.002	2	2000
$\pi\pi f_2$,$K\bar{K}f_2$, s–channel f_2 exch.	0.020	2	2000

TABLE IV. Parameters used in the $K\bar{K} \to K\bar{K}$ potential.

Vertex $\alpha\beta\gamma$	Coupling Constant $\frac{g^2_{\alpha\beta\gamma}}{4\pi}$	Form factor power $n_{\alpha\beta\gamma}$	Cutoff $\Lambda_{\alpha\beta\gamma}$ (MeV)
$K\bar{K}\rho$, t–channel ρ exch.	0.525	2	3100
$K\bar{K}\omega$, t–channel ω exch.	-0.525	2	3100
$K\bar{K}\phi$, t–channel ϕ exch.	-1.050	2	3100
$K\bar{K}\rho$, s–channel ρ exch.	0.525	2	3100
$K\bar{K}\epsilon$, s–channel ϵ exch.	0.001	2	2000
$K\bar{K}f_2$, s–channel f_2 exch.	0.010	2	2000

TABLE V. Parameters used in the $N\bar{N} \to \pi\pi, K\bar{K}$ transition potentials: t channel baryon exchanges.

Vertex $\alpha\beta\gamma$	Coupling Constant $\frac{f^2_{\alpha\beta\gamma}}{4\pi}$	Form factor power $n_{\alpha\beta\gamma}$	Cutoff $\Lambda_{\alpha\beta\gamma}$ (MeV)
$NN\pi$	0.0790	1	1780
$N\Delta\pi$[a]	0.36	2	1705
$N\Lambda K$	0.0718	1	2500
$N\Sigma K$	0.00247	1	2500

[a] $x_\Delta = -0.847$

TABLE VI. The scattering lengths and volumes in units $m_\pi^{-(2L+1)}$.

	model	Koch and Pietarinen [18]
S_{11}	0.165	0.173 ± 0.003
S_{31}	–0.092	–0.101 ± 0.004
P_{11}	–0.080	–0.081 ± 0.002
P_{31}	–0.042	–0.045 ± 0.002
P_{13}	–0.029	–0.030 ± 0.002
P_{33}	0.210	0.214 ± 0.002

This figure "fig1-1.png" is available in "png" format from:

http://arXiv.org/ps/nucl-th/9411022v1

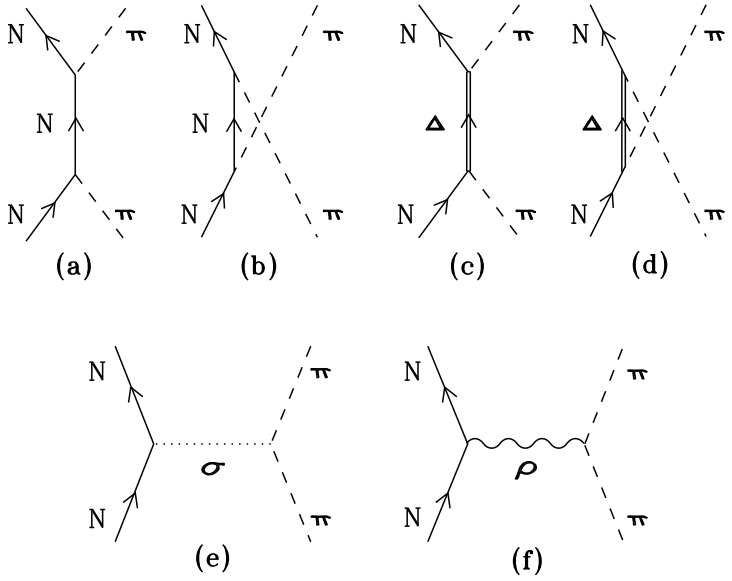

C. Schuetz et al., Fig. 1

This figure "fig2-1.png" is available in "png" format from:

http://arXiv.org/ps/nucl-th/9411022v1

This figure "fig1-2.png" is available in "png" format from:

http://arXiv.org/ps/nucl-th/9411022v1

This figure "fig2-2.png" is available in "png" format from:

http://arXiv.org/ps/nucl-th/9411022v1

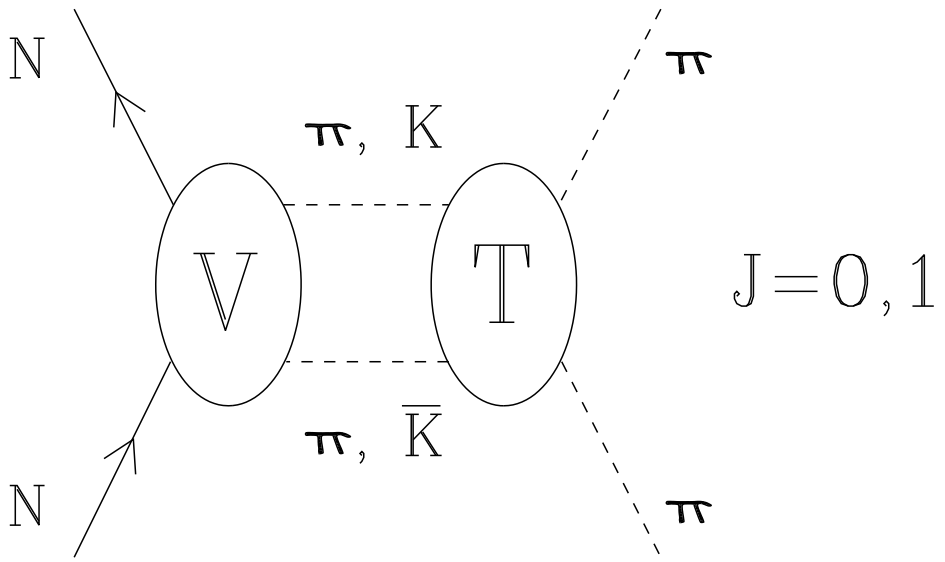

C. Schuetz et al., Fig. 2

This figure "fig1-3.png" is available in "png" format from:

http://arXiv.org/ps/nucl-th/9411022v1

This figure "fig2-3.png" is available in "png" format from:

http://arXiv.org/ps/nucl-th/9411022v1

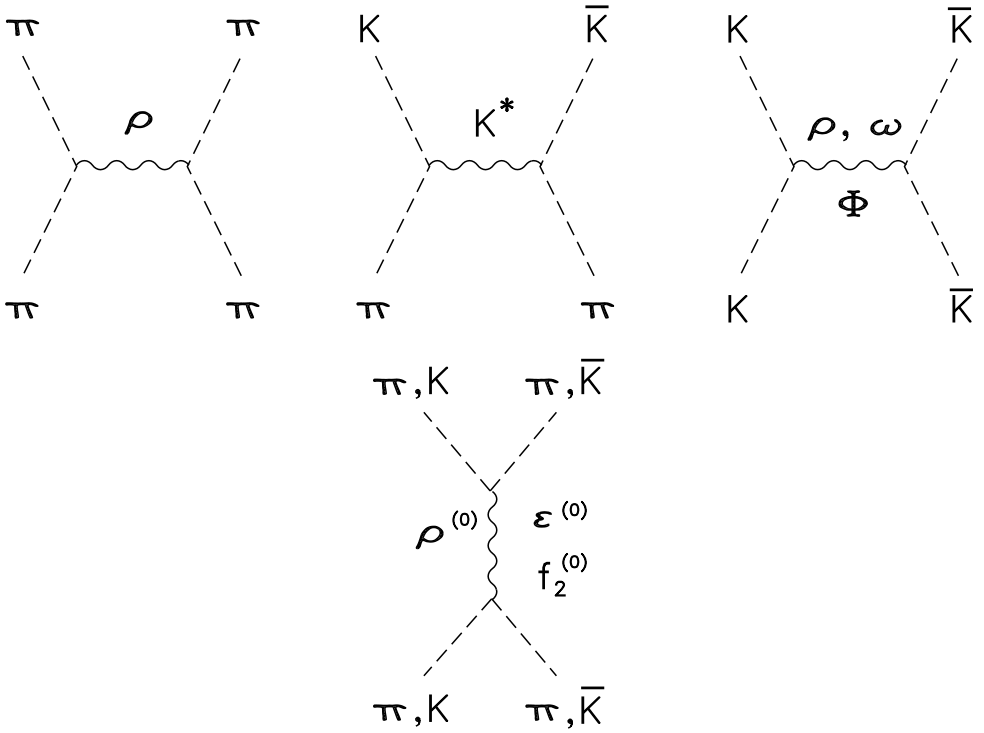

C. Schuetz et al., Fig. 3

This figure "fig1-4.png" is available in "png" format from:

http://arXiv.org/ps/nucl-th/9411022v1

This figure "fig2-4.png" is available in "png" format from:

http://arXiv.org/ps/nucl-th/9411022v1

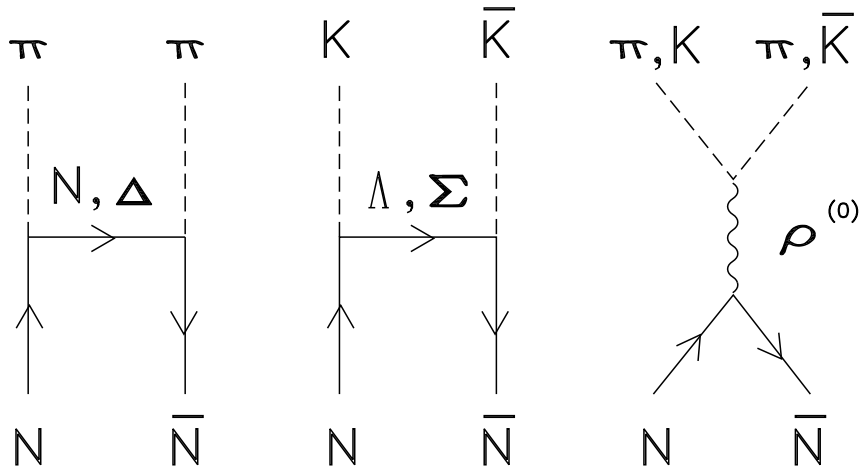

C. Schuetz et al., Fig. 4

This figure "fig1-5.png" is available in "png" format from:

http://arXiv.org/ps/nucl-th/9411022v1

This figure "fig2-5.png" is available in "png" format from:

http://arXiv.org/ps/nucl-th/9411022v1

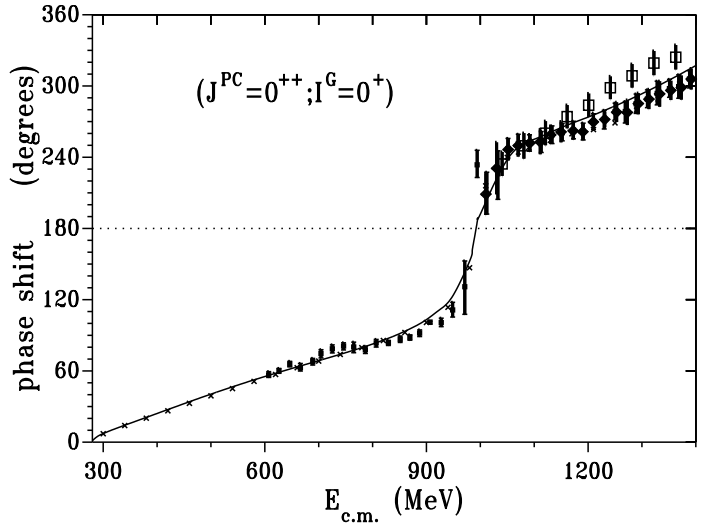

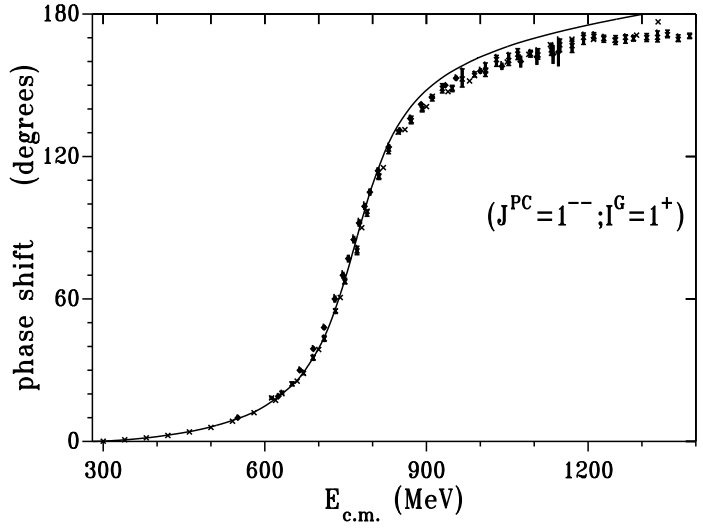

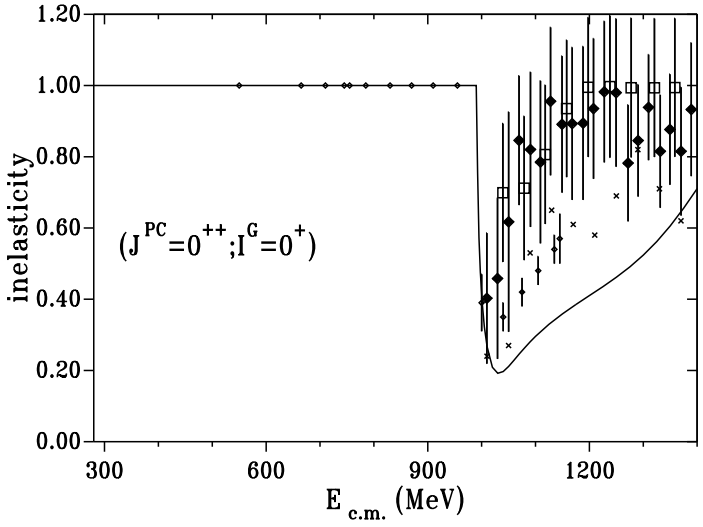

C. Schuetz et al., Fig. 5

This figure "fig2-6.png" is available in "png" format from:

http://arXiv.org/ps/nucl-th/9411022v1

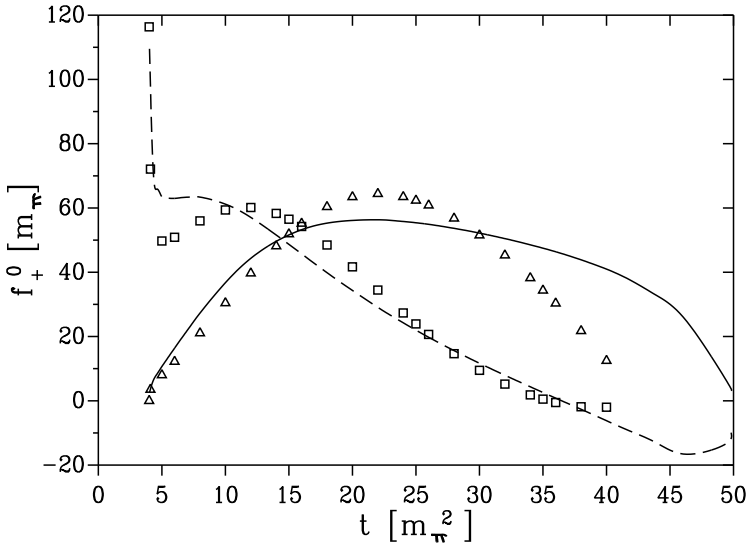

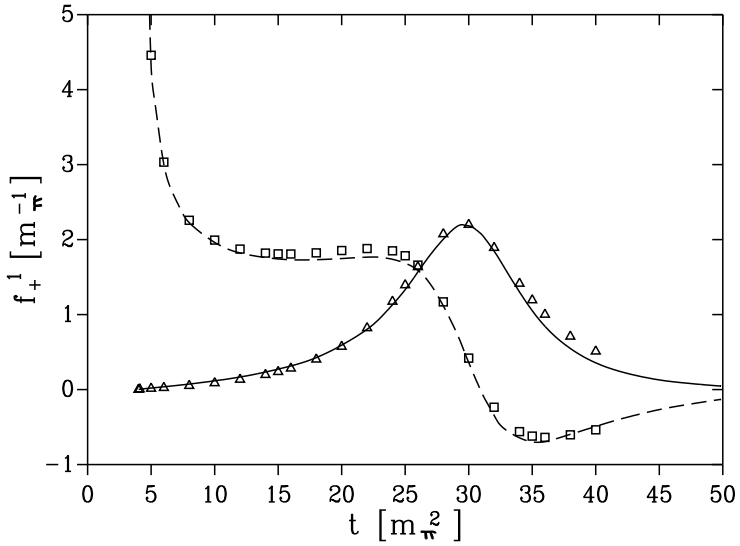

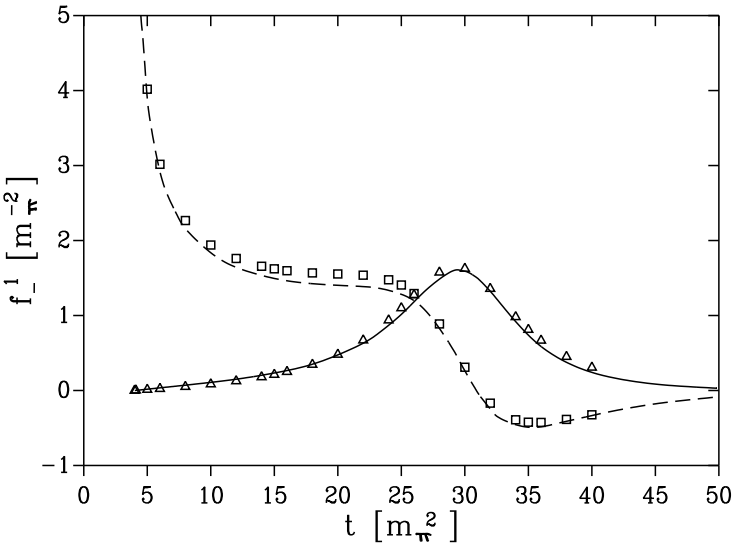

C. Schuetz et al., Fig. 6

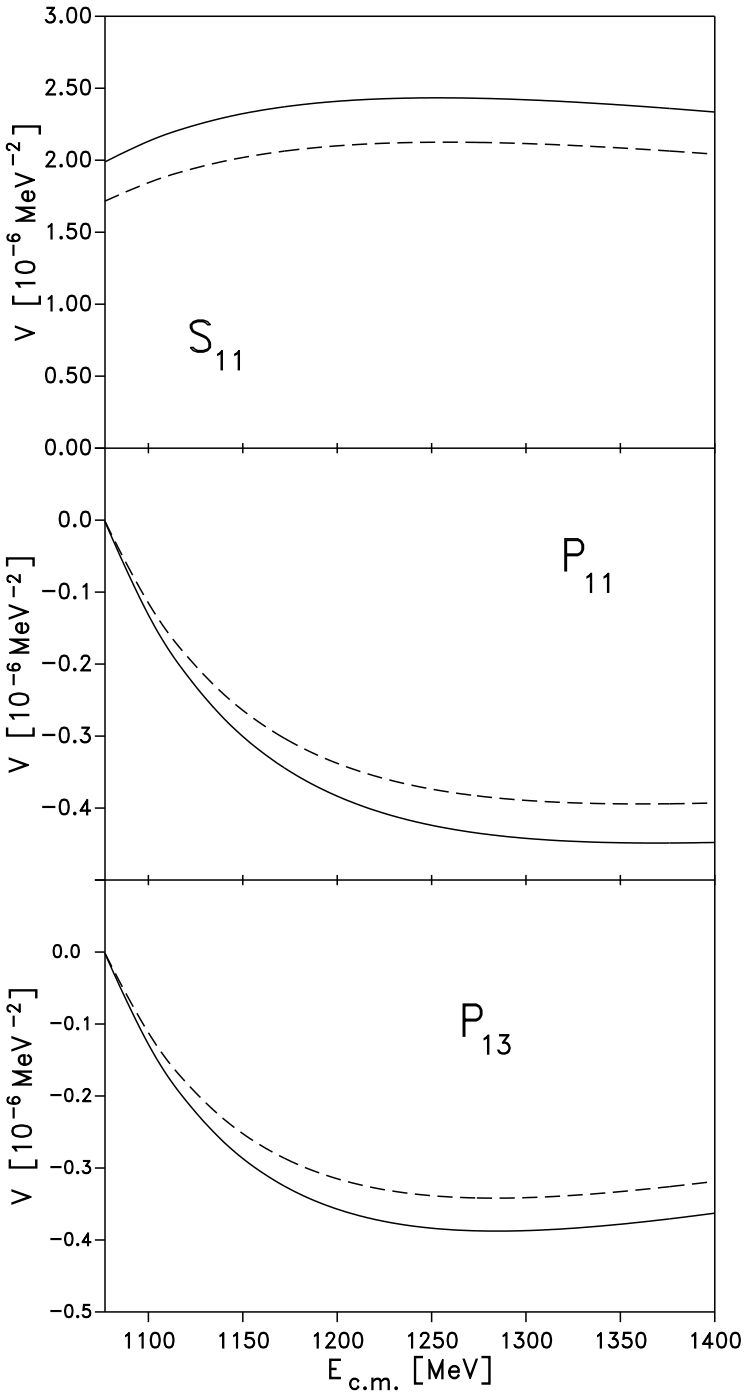

C. Schuetz et al., Fig. 7

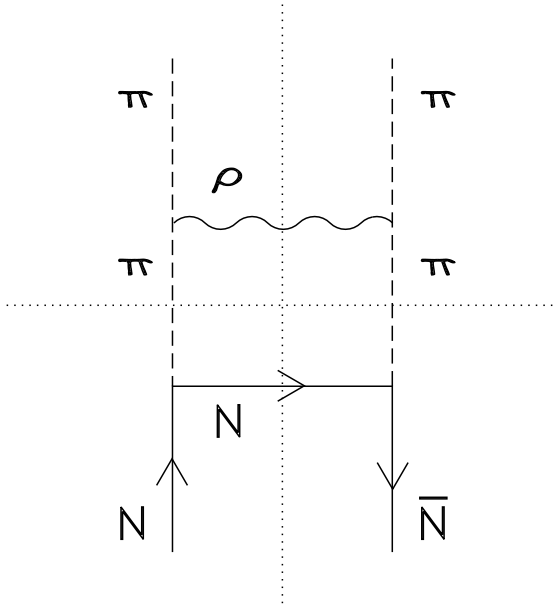

C. Schuetz et al., Fig. 8

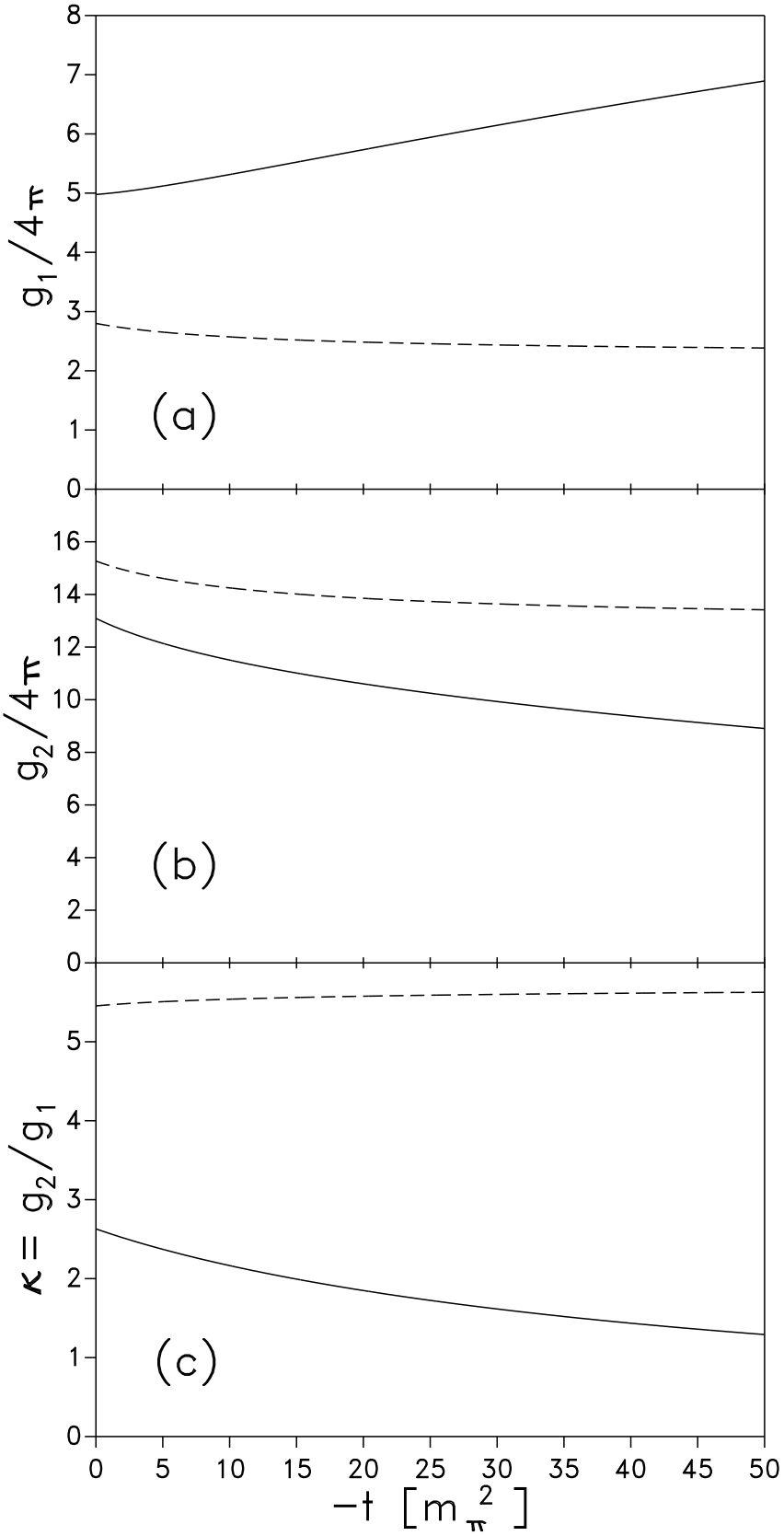

C. Schuetz et al., Fig. 9

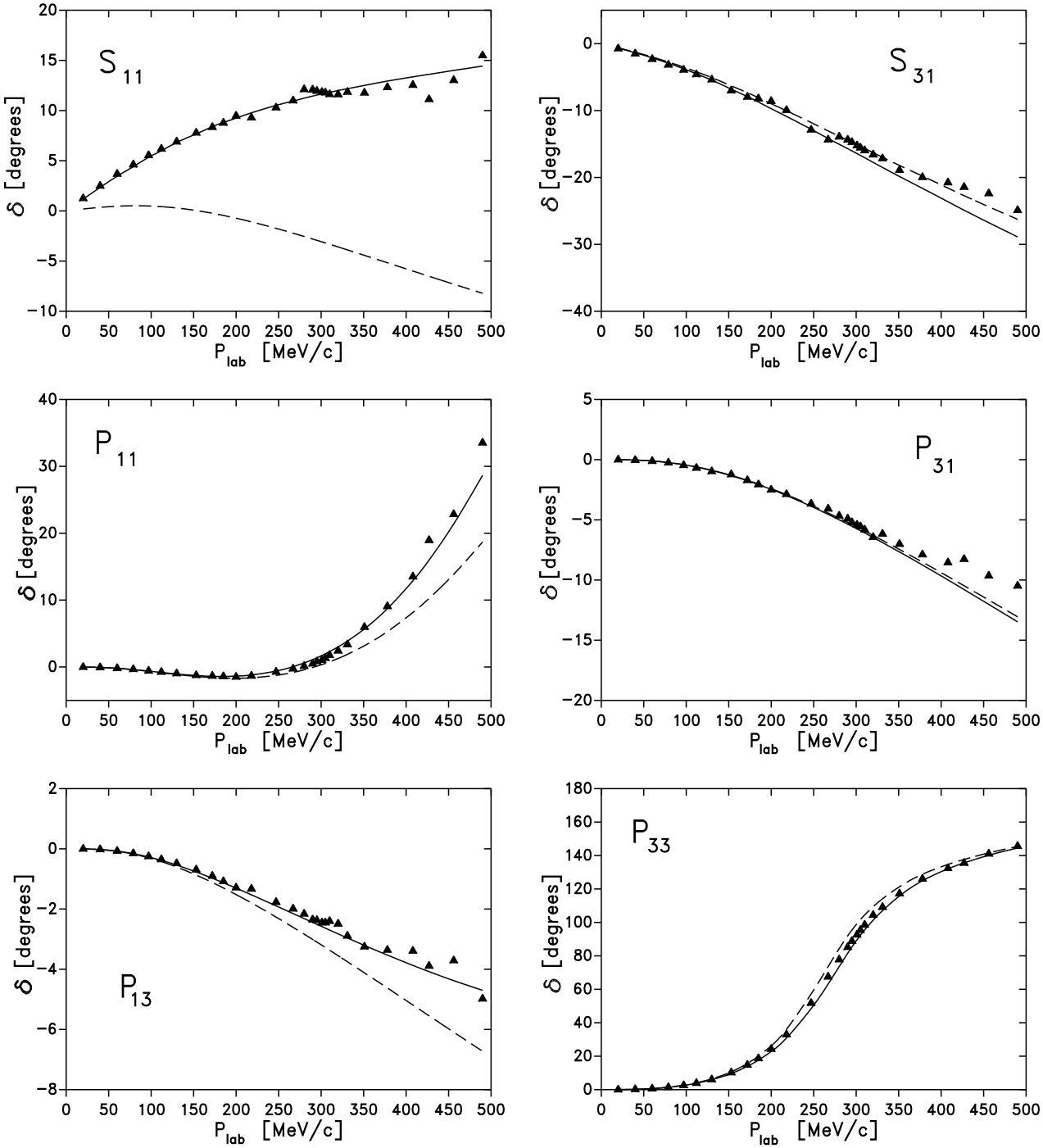

C. Schuetz et al., Fig. 10

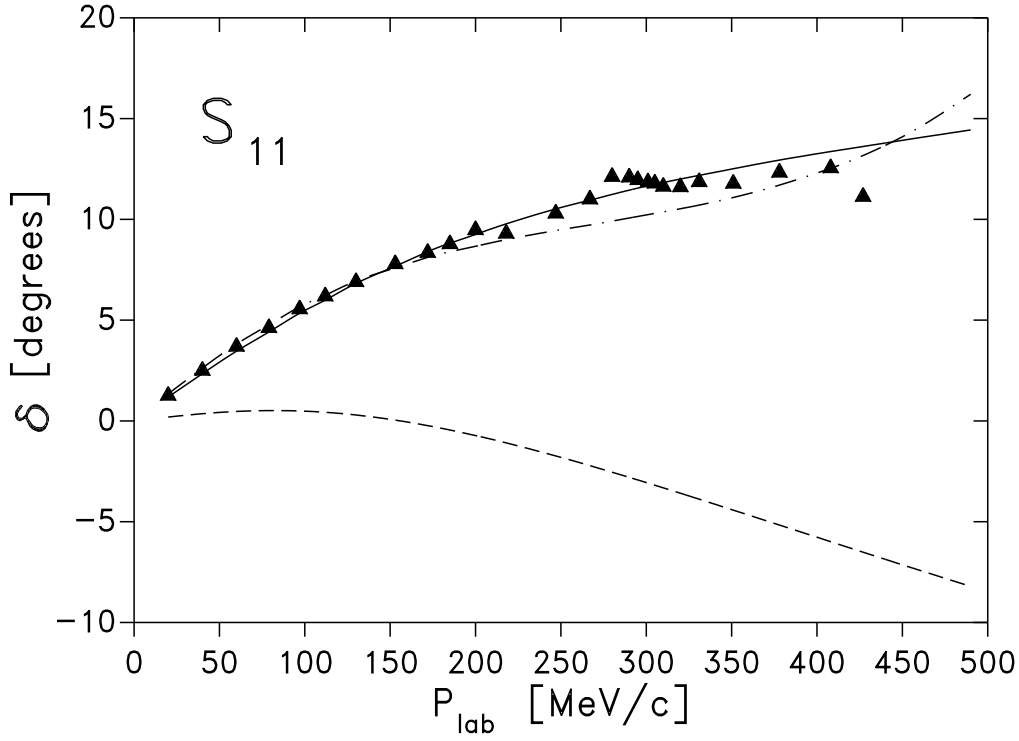

C. Schuetz et al., Fig. 11